NASA/TM–20260004532

Micromechanical Design of Carbon Nanotube Ribbon Reinforced Polymer Composite Materials

Benjamin D. Jensen, Godfrey Sauti, John M. Gardner, Russell A. Wincheski, Scott R. Zavada, Emilie J. Siochi
Langley Research Center, Hampton, Virginia

Jae-Woo Kim
Analytical Mechanics Associates, Hampton, Virginia

May 2026

NASA STI Program Report Series

Since its founding, NASA has been dedicated to the advancement of aeronautics and space science. The NASA scientific and technical information (STI) program plays a key part in helping NASA maintain this important role.

The NASA STI Program operates under the auspices of the Agency Chief Information Officer. It collects, organizes, provides for archiving, and disseminates NASA's STI. The NASA STI Program provides access to the NTRS Registered and its public interface, the NASA Technical Report Server, thus providing one of the largest collections of aeronautical and space science STI in the world. Results are published in both non-NASA channels and by NASA in the NASA STI Report Series, which includes the following report types:

- TECHNICAL PUBLICATION. Reports of completed research or a major significant phase of research that present the results of NASA programs and include extensive data or theoretical analysis. Includes compilations of significant scientific and technical data and information deemed to be of continuing reference value. NASA counterpart of peer-reviewed formal professional papers, but having less stringent limitations on manuscript length and extent of graphic presentations.

- TECHNICAL MEMORANDUM. Scientific and technical findings that are preliminary or of specialized interest, e.g., quick release reports, working papers, and bibliographies that contain minimal annotation. Does not contain extensive analysis.

- CONTRACTOR REPORT. Scientific and technical findings by NASA-sponsored contractors and grantees.

- CONFERENCE PUBLICATION. Collected papers from scientific and technical conferences, symposia, seminars, or other meetings sponsored or co-sponsored by NASA.

- SPECIAL PUBLICATION. Scientific, technical, or historical information from NASA programs, projects, and missions, often concerned with subjects having substantial public interest.

- TECHNICAL TRANSLATION. English-language translations of foreign scientific and technical material pertinent to NASA's mission.

Specialized services also include organizing and publishing research results, distributing specialized research announcements and feeds, providing information desk and personal search support, and enabling data exchange services.

For more information about the NASA STI Program, see the following:

- Access the NASA STI program home page at `http://www.sti.nasa.gov`

- Help desk contact information: `https://www.sti.nasa.gov/sti-contact-form/` and select the "General" help request type.

NASA/TM–20260004532

Micromechanical Design of Carbon Nanotube Ribbon Reinforced Polymer Composite Materials

Benjamin D. Jensen, Godfrey Sauti, John M. Gardner, Russell A. Wincheski, Scott R. Zavada, Emilie J. Siochi
Langley Research Center, Hampton, Virginia

Jae-Woo Kim
Analytical Mechanics Associates, Hampton, Virginia

National Aeronautics and
Space Administration

Langley Research Center
Hampton, Virginia 23681-2199

May 2026

Acknowledgments

This work was funded through the Super-lightweight Aerospace Composites project under the NASA Space Technology Mission Directorate Game Changing Development Program.

Available from:

NASA STI Program / Mail Stop 150
NASA Langley Research Center
Hampton, VA 23681-2199

Abstract

Lightweight materials are an important component of the design of aerospace structures. Carbon nanotube materials have been considered for this purpose due to the strength and stiffness of individual nanotubes, and the commercial availability of bulk formats such as fibers. These fibers can have a ribbon cross section which results in a different design space for their composites relative to traditional reinforcements which have a round cross section. This work applies brick-and-mortar micromechanical models and classical lamination theory with an inverse approach to investigate the design space of these composites. Using this approach, the influences of fiber geometry and axial and transverse mechanical properties are mapped. Finally, a sensitivity study is performed and the relative impacts of $\pm 10\%$ variations in the constituent material and geometric properties are ranked. Lamina axial moduli were found to range from a maximum of 3x to 1x minimum relative to a target quasi-isotropic laminate modulus depending on the anisotropy and shear modulus of the lamina. The fiber targets depended strongly on the fiber volume fraction in the lamina and the fiber axial modulus target was found to range from 4.8x to 3.2x the quasi-isotropic laminate target. The sensitivity analysis found that the largest driver of performance was the volume fraction, followed by the fiber axial modulus. While bio-based brick-and-mortar composites, such as nacre, can benefit from reinforcement aspect ratios above 10, for carbon nanotube ribbon (or carbon fiber)/polymer composites the sensitivity study indicated that the optimal cross-sectional aspect ratio was relatively smaller, potentially less than three.

Contents

1 Introduction

Advances in lightweight structural materials are important for aerospace applications where reductions in the structural mass budget for payloads or vehicles can allow more mass for scientific instruments and enable new mission designs [1]. Carbon nanotubes have been considered as reinforcement in polymer matrix composites due to the strength and stiffness of individual nanotubes, and the commercial availability of bulk nanotube formats such as fibers, sheets, and pulp [2–4].

Carbon nanotube fibers are commercially available in a format with a ribbon cross section [5]. Most commercial fiber reinforcements have a circular cross section due to manufacturability, cost, and performance reasons [6]. For example, surface tension of wet-spun fibers drives them into circular cross sections. Stabilization and pyrolysis steps in the manufacture of carbon fibers are dominated by diffusion processes that can also benefit from even diffusion through a circular cross section. Despite the ubiquity of circular cross section reinforcing fibers, there have been academic investigations of ribbon, kidney, C-shape, hollow, triangular, star, and other crenulated and irregular cross section reinforcements [7–12] and limited commercialization [13]. Because of the ubiquity of round fiber reinforcements, general micromechanical analysis used in the design of laminates is formulated around the presumption of round fibers. While micromechanical treatments of ribbon reinforced composites have been developed [14–16], the broader analysis of ribbon fiber composites has remained limited.

Recently developed methods for the manufacture of high-strength carbon nanotube fibers using a continuous aerogel-spinning process from a floating-catalyst chemical vapor deposition furnace yield fibers with a ribbon cross section [5, 17]. An example of a composite made from these fibers is shown in Figure 1. While carbon fibers have a turbostratic microcrystalline graphitic internal structure and diameters of around 7 µm, the structure of floating-catalyst chemical vapor deposition carbon nanotube fibers is nanotube bundle networks. The cross-sectional dimensions of the carbon nanotube ribbons can be controlled though the manufacturing process and in Figure 1 are approximately 15 µm by 100 µm. Analysis that explores the lamina design space with ribbon fibers is important for optimizing the nanotube fiber and understanding the impact of fiber geometry and mechanical properties on composite lamina and laminate properties.

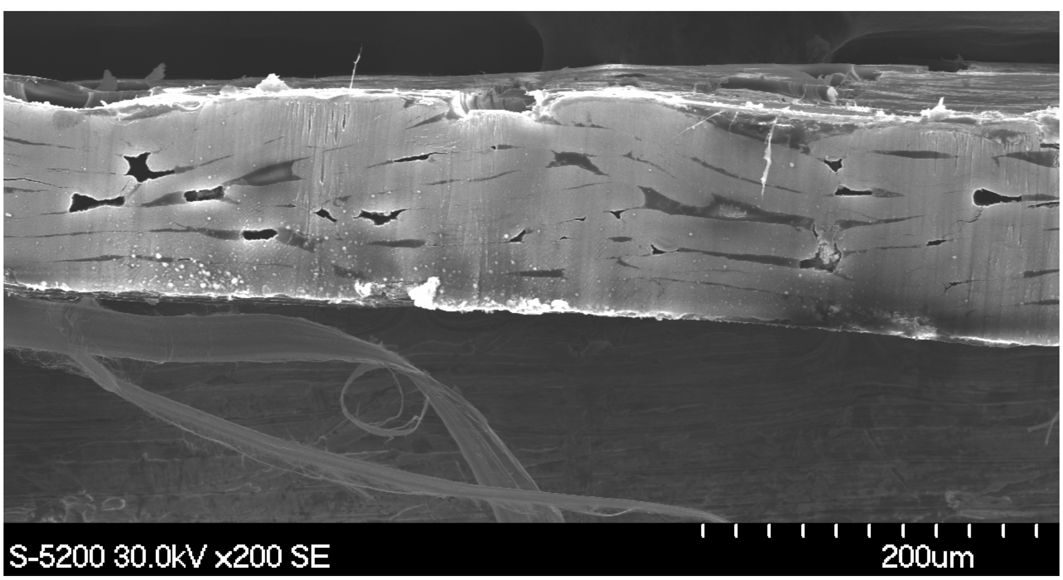

Figure 1. Cross sectional view of a composite made from carbon nanotube fibers with ribbon cross section.

The elongated cross section of the nanotube fibers results in a mix of shear load transfer (along the width of the fiber) and load transfer normal to the fiber edge ends. The relative contribution of shear and normal load transfer is expected to depend on the fiber aspect ratio and mechanical performance of the fiber relative to the matrix. The behavior of transversely loaded continuous ribbon fibers are analogous to discontinuous fibers loaded in the axial direction. Round fibers that compose typical composites have a cross-sectional aspect ratio of one, and therefore experience negligible shear load transfer.

There have been a number of investigations using micromechanical and other numerical methods to understand the behavior of brick-and-mortar composites for bio-based, bio-mimic, and other composite materials [18–23]. Nacre and nacre-inspired materials contain a ceramic "brick" connected by protein or other soft organic material "mortar" and have been extensively studied, including the development of micromechanical models [24–27]. Because the mechanical properties of the ceramic and protein constituents differ from those of carbon fiber and carbon nanotube materials, the conclusions that have been drawn from studies of ceramic/protein composites should not be indiscriminately applied to carbon-nanotube-fiber composites. This is not due to any incompatibility of the micromechanics, but rather the vast difference in the design space of interest, which arises from the relative similarity of the constituent properties in nanotube-fiber-reinforced polymer composites relative to ceramic/protein composites.

Micromechanical analysis of carbon-based composites is typically performed starting with the properties of a handful of commercially available constituent materials and working up through the lamina and laminate length-scales to determine a laminate layup that meets a target load requirement [28]. Often this is performed automatically using structural sizing software [29]. In this work, we approach the micromechanics from a material design standpoint, sometimes referred to as an inverse approach, starting with a notional laminate and working backwards to design materials that meet the target requirements. With this approach we are also able to perform a sensitivity study and identify material properties that are most critical in meeting a laminate target.

This report explores carbon-nanotube-fiber-reinforced composites in the linear elastic material behavior regime using micromechanics models developed for brick-and-mortar composites combined with classical lamination theory. The analysis explores the design space of laminates fabricated with ribbon fibers. The resulting analysis is intended to reduce the scope of composite fabrication options and estimate the impact of trade-offs that need to be made at the laminate and lamina level. These simple models provide guidance quickly that explore extreme boundaries of the problem and can be subsequently refined as warranted.

2 Micromechanical Framework

2.1 Carbon-nanotube-fiber-reinforced polymer-matrix composite unit cells

A schematic of a quasi-isotropic laminate with carbon nanotube ribbons is shown in Figure 2. The cross section of the fibers in the 0° and 90° lamina are highlighted in red. A schematic of an idealized lamina composed of carbon nanotube ribbons compared to the more typical round fiber is depicted in Figure 3. The maximum fiber volume fraction that hexagonally packed round fibers can reach is $\sqrt{3}\pi/6 \approx 0.9$, as indicated with teal in Figure 3. This limit occurs when the fibers are in direct contact, leaving only the quasi-triangular spaces between fibers for polymer. For a fiber volume fraction of 0.6, the spacing between fibers becomes $\approx 0.23D$, where D is the fiber diameter.

For ribbon fibers, the lamina in the transverse direction resembles a brick-and-mortar structure or an aligned discontinuously reinforced composite. However, the nanotube-fiber-reinforced lamina departs from these analogues in important ways. Brick-and-mortar composites are typically composed of flakes, instead of long fibers. Analyses of discontinuous composites also assume the discontinuity is in the axial direction of

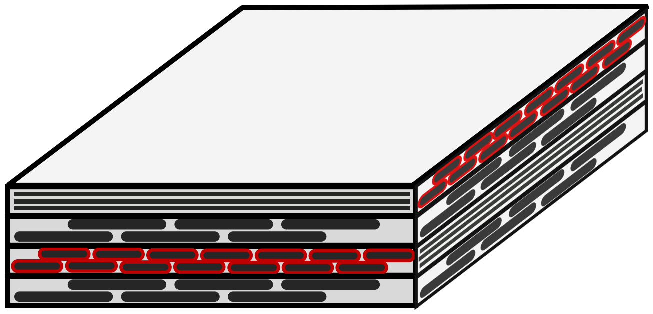

Figure 2. Schematic of the top half of a [90°/45°/0°/-45°]s quasi-isotropic laminate with ribbon fiber reinforcement within the lamina. Cross sections normal to the fiber axis are outlined in red.

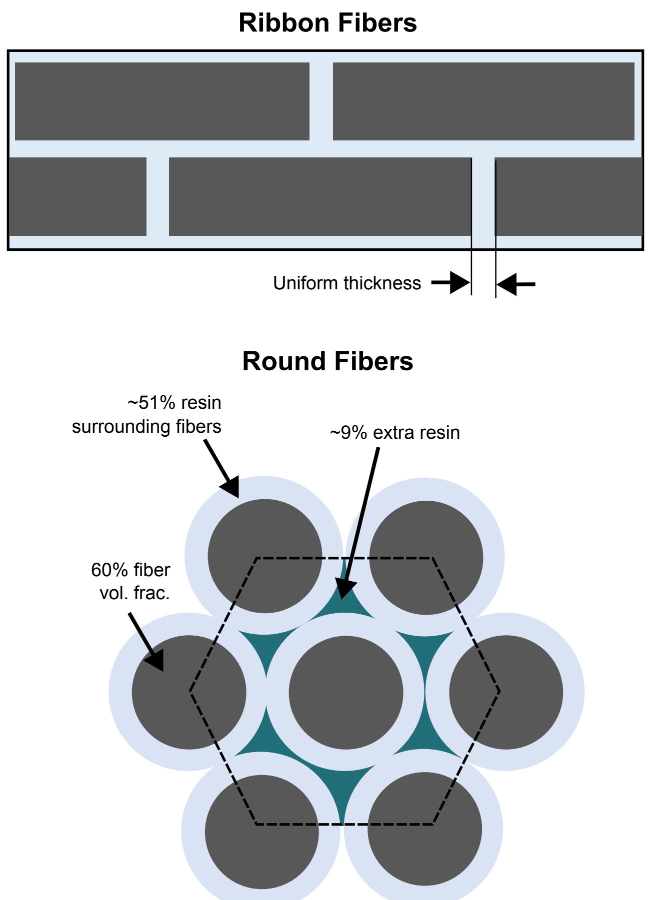

Figure 3. Comparison of ideal cross-sectional unit cells for ribbon fiber composite laminae and round fiber composite laminae.

the fiber and not, as is the case here, in the fiber transverse direction. Despite these important differences in lamina structure, the mechanics is similar, e.g., transverse loading of ribbon fiber composites is similar to axial loading of discontinuous fiber composites, or traditional brick-and-mortar composites. For these structures, shear load transfer to the reinforcement plays an important role in the material response.

In this work, the relationships between laminate and lamina properties are described following classical lamination theory, as described in Reference [30]. In classical lamination theory, the lamina are represented as two dimensional, transversely isotropic materials.

2.2 Micromechanical description of lamina

The engineering constants for lamina can be estimated from the reinforcement and matrix properties. The axial Young's modulus of the lamina, E_1, can be approximated following a rule of mixtures of the fiber and matrix

$$E_1 = V_f E_{f1} + (1 - V_f) E_m \quad (1)$$

where V_f is the fiber volume fraction, E_{f1} is the fiber axial Young's modulus, and E_m is the matrix Young's modulus. The assumption for the rule of mixtures includes that strains are equal in the fiber and matrix and that the properties of the fiber and matrix do not change when combined into a composite. For a typical composite fiber volume fraction of 0.6, this relationship works well. It is typical to compute E_{f1} and E_m independently and use them in the rule of mixtures. For most composites this is a reasonable approach because the properties of the matrix and fiber do not appreciably change when combined into a composite material. However, if the fiber or matrix does change behavior after composite fabrication, E_{f1} and E_m will reflect the properties of the constituents within the composite. This relationship might diverge from experimental results for extreme fiber volume fractions which are more easily achieved with brick-and-mortar structures, compared to traditional round-fiber composites, as shown in Figure 3. If the distance between fibers approaches the thickness of the structured matrix interphase, the modulus of this interface may differ from the bulk phase measured in isolation. Similarly, the surface of carbon nanotube fibers can be slightly porous and the matrix may infiltrate a small distance – somewhat strengthening the outer skin of the fiber [31].

The transverse modulus, E_2, for composites with round fibers is typically approximated with an inverse rule of mixtures $1/E_2 = V_f/E_{f2} + (1 - V_f)/E_m$ where E_{f2} is the transverse modulus of the fiber. The assumption here is that stresses (instead of strains) are equal in the fiber and matrix. However, for nanotube fibers that have a ribbon shape, this assumption is not appropriate. For ribbon fibers loaded in the transverse direction, a shear-lag load transfer behavior is expected, where the stress at the sides of the fiber is lowest, and increases toward the center of the fiber as depicted in Figure 4.

To better approximate the lamina transverse Young's modulus, the following relationship from Reference [32] is used where ρ is the aspect ratio of the ribbon fiber cross section and G_m is the matrix shear modulus.

$$E_2 = -\frac{E_{f2} G_m V_f^2 \rho^2}{4E_{f2}\,(V_f - 1) - 4/3 \cdot G_m V_f \rho^2} \quad (2)$$

In this work, this equation has been used to model ribbon reinforcements in a brick-and-mortar configuration, similar to the geometry of the nanotube fibers. This equation relates the transverse Young's modulus of the fiber, shear modulus of the matrix, and geometry of the fiber. It assumes that there is no load transfer between the side ends of the fibers and the matrix and that the load is transferred along the long edge of the fibers.

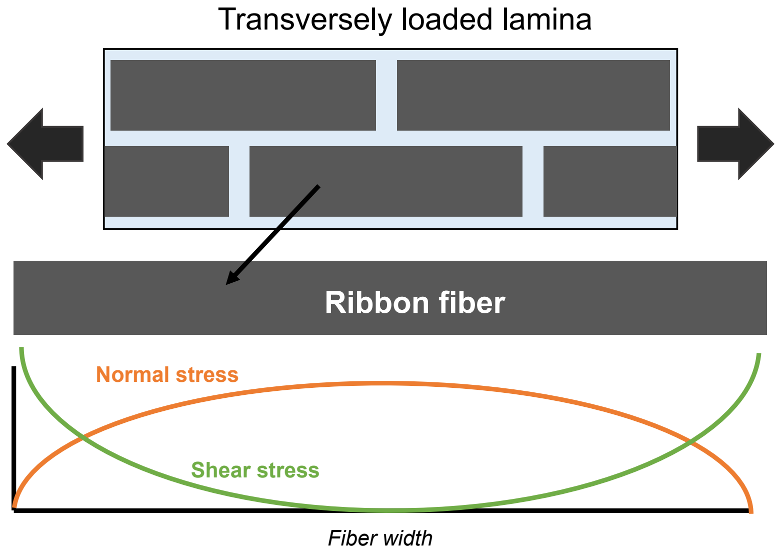

Figure 4. Notional normal and shear stresses along a ribbon fiber within a lamina loaded in the transverse direction.

The lamina shear modulus (G_{12}) is computed using an inverse rule of mixtures and Poisson's ratio (ν_{12}) is computed using a rule of mixtures

$$\frac{1}{G_{12}} = \frac{V_f}{G_{f12}} + \frac{1 - V_f}{G_m} \tag{3}$$

$$\nu_{12} = V_f \nu_{f12} + (1 - V_f)\,\nu_m \tag{4}$$

where G_{f12} is the fiber shear modulus, ν_{f12} is the fiber Poisson's ratio, and ν_m is the matrix Poisson's ratio.

In summary, to predict the lamina linear elastic behavior, six material constants and two geometric inputs are required. Because the matrix is isotropic, there are only two independent material constants which are related to the third dependent material constant through $G_m = E_m/[2(1 + \nu_m)]$. The fibers are treated as transversely isotropic, requiring four material constants: E_{f1}, E_{f2}, G_{f12}, ν_{f12}. The geometric parameters are the fiber aspect ratio (ρ) and the lamina fiber volume fraction (V_f).

By selecting reasonable ranges for each material property, the design space for laminates composed of carbon nanotube ribbons can be established and the sensitivity of the various material and geometric parameters can be evaluated to aid the design of the nanotube fibers and their composites.

3 Lamina requirements to reach laminate targets

For this work, a quasi-isotropic (QI) symmetric laminate is selected as the target system. A QI laminate is defined as a laminate with [A] that is of an isotropic form, where [A] refers to the in-plane response block of the ABD matrix from classical lamination theory [30]. The ABD matrix is a block matrix that relates force and moment resultants to mid-plane strains and curvatures where the [A] block governs in-plane response, [B] captures extension–bending coupling, and [D] governs bending response. An isotropic [A] has two independent material constants and has the form below. Note that [A] is exactly isotropic and "quasi" does not refer to a mild anisotropy in [A]. Therefore, in-plane extension and shear for QI laminates are rotationally invariant. A laminate with three or more lamina of the same material that are evenly oriented will result in an isotropic $[A]$ [28]. For example, laminates with layup [60°/0°/-60°]s and [0°/45°/-45°/90°]s are QI and have identical $[A]$ (assuming the laminates are the same thickness). The extra lamina in the second example does not affect the laminate engineering constants. Therefore, in this work the specific layup of QI laminates is not provided, as the results apply to any laminate with isotropic $[A]$.

3.1 Lamina requirements to reach a QI laminate target

The independent lamina properties that can be modified to meet a QI laminate axial modulus (E_{QI}) are the lamina axial modulus (E_1), lamina transverse modulus (E_2), lamina in-plane shear modulus (G_{12}), and lamina in-plane Poisson's ratio (ν_{12}). An initial screening analysis indicated that ν_{12} has a relatively minor impact on E_{QI}. Therefore, a typical ν_{12} of 0.25 was selected and the effect of the remaining lamina properties is shown in Figure 5. In Figure 5, the lamina E_1 has been normalized relative to the laminate E_{QI}, thereby indicating how much higher E_1 must be than the E_{QI} target. Similarly, E_2 is normalized against E_1 and indicates the degree of anisotropy of the lamina. G_{12} is also normalized against E_1. The upper limit of $G_{12}/E_1 = 0.5$ corresponds to that of an isotropic material, which the lamina are unlikely to exceed.

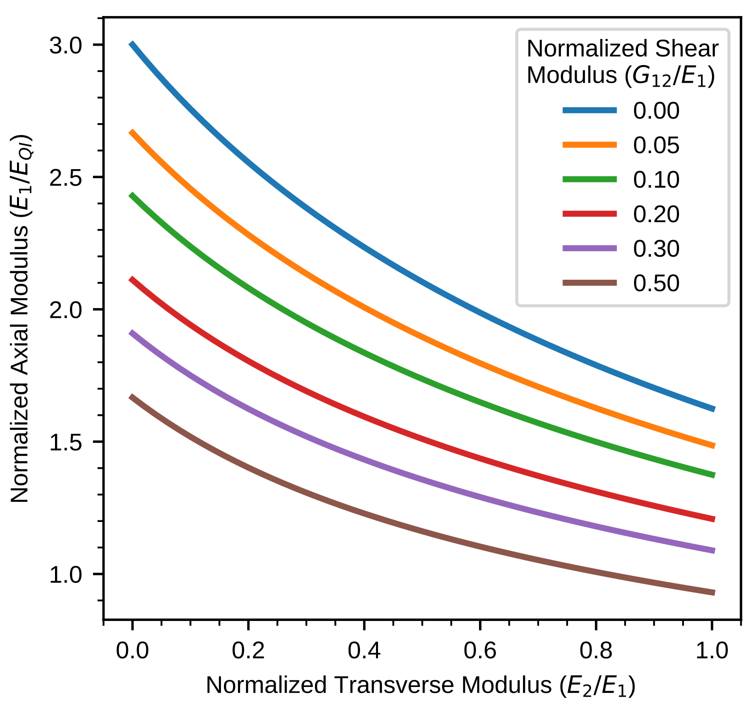

Figure 5. Lamina properties required to reach a target laminate Young's modulus, with $\nu_{12} = 0.25$.

In Figure 5, the ratio of transverse to axial modulus (E_2/E_1) is shown on the x-axis ranging from zero, where the transverse modulus makes no contribution to laminate stiffness, to 1, representing an isotropic material. The curve for $G_{12}/E_1 = 0$ (blue) represents a lower bound in which there is no shear contribution to the laminate mechanical performance. The upper bound for shear stiffness is shown in brown where $G_{12}/E_1 = 0.5$, which represents an isotropic material. In the limit of poor transverse and shear moduli, the lamina axial modulus may be required to be as much as 3x higher than the target QI laminate axial modulus. Lamina engineering constants for some composite lamina are provided in Table 1. As G_{12}/E_1 increases to 0.05, a value typical of carbon-fiber-reinforced polymer composites, the axial lamina modulus required drops ∼11% to 2.7x higher than the QI target. If the lamina shear modulus can be increased to $G_{12}/E_1 = 0.1$, the maximum lamina E_1 required drops to 2.4x the QI target.

At the other extreme, of a more isotropic lamina, values from carbon nanotube sheets (which are two-dimensional like a lamina, but do not contain a matrix) are provided in Table 2. These sheets can have a mild orientation along the direction of manufacture, resulting in $E_2/E_1 > 0.75$. For these sheets, the maximum E_1/E_{QI} that may be required is 1.7x, assuming no shear contribution, and approaches 1x as the lamina becomes isotropic. Some of the nanotube materials were processed using spark plasma sintering (SPS) to enhance their mechanical properties [33]. Also known as field assisted sintering technique (FAST), SPS is a process where pulsed DC currents are passed through a material while it is compressed between graphite dies under vacuum. For SPS processed CNT sheets, both axial and transverse moduli increased. However, the increase in transverse modulus was relatively higher than the axial modulus resulting in larger E_2/E_1 ratios.

Table 1. Lamina engineering constants for several composites

Material	**Description**	**Normalized transverse modulus (E_2/E_1)**	**Normalized shear modulus (G_{12}/E_1)**	**Poisson's ratio (ν_{12})**	**Ref.**
Infiltrated Nanocomp carbon nanotube/BMI	composite fiber/BMI	12%	-	-	[5]
Hexcel® IM7/8552	carbon fiber/epoxy	5.5%	2.9%	0.31	[34]
Thornel® T-300/934	carbon fiber/epoxy	7.9%	5.3%	0.22	[28]
Hercules AS/3501	carbon fiber/epoxy	6.5%	5.0%	0.3	[28]
Thornel® P-100/ERL 1962	pitch carbon fiber/epoxy	1.3%	1.2%	0.31	[28]
Kevlar® 49/934	aramid/epoxy	7.3%	3.0%	0.34	[28]
Scotchply® 1002	E-glass/epoxy	21%	10%	0.26	[28]
Rigidite™/5505	boron/epoxy	9.1%	2.7%	0.23	[28]
Spectra® 900/826	polyethylene/epoxy	11%	4.7%	0.32	[28]
E-glass/470-36	E-glass/vinylester	28%	11%	0.32	[28]

3.2 [0°/90°]s laminate lamina requirements to reach an equivalent QI laminate target

Dropping one ply, from three (or more) to two evenly spaced plies, results in a laminate that is not QI. This two layer laminate is modeled with a [0°/90°]s layup. The modulus of a [0°/90°]s laminate along various loading directions (ϕ) is shown in Figure 6(a) with $G_{12}/E_1 = 0.05$, which is typical for oriented fiber lamina. In Figure 6(a)(b), the modulus is normalized against a target QI laminate, so that the Young's modulus at 45° has a value of one. As the laminate is rotated closer to the fiber directions (0° and 90°) the modulus exceeds the QI laminate target value, representing an excess capacity in those directions. Depending on the relative performance in the transverse direction the amount of excess capacity increases from 3x to 5.4x with the excess capacity increasing with increasing transverse ratio. This is because the properties at 45° are dominated by G_{12} and increases in the fiber directions to not substantially affect the off-axis modulus. Designing a [0°/90°]s laminate with properties similar to a QI panel requires lamina with G_{12} that approaches an isotropic material. An example of this is shown in Figure 6(b) where $G_{12}/E_1 = 0.3$, representing a substantially more isotropic lamina material. In this case the maximum excess modulus is approximately 1.2x for the most isotropic E_2/E_1 case ($E_2/E_1 = 1$).

Looking at the properties of the [0°/90°]s laminate along the 45° direction, the knockdown relative to the lamina axial modulus is shown in Figure 6(c). From Figure 6(c), it can be seen that the in-plane shear modulus of the lamina plays a critical role in the laminate response at 45°. As the material becomes more isotropic and G_{12} approaches the limit of $E/[2(1+\nu)]$ the transverse modulus plays a larger role in the response.

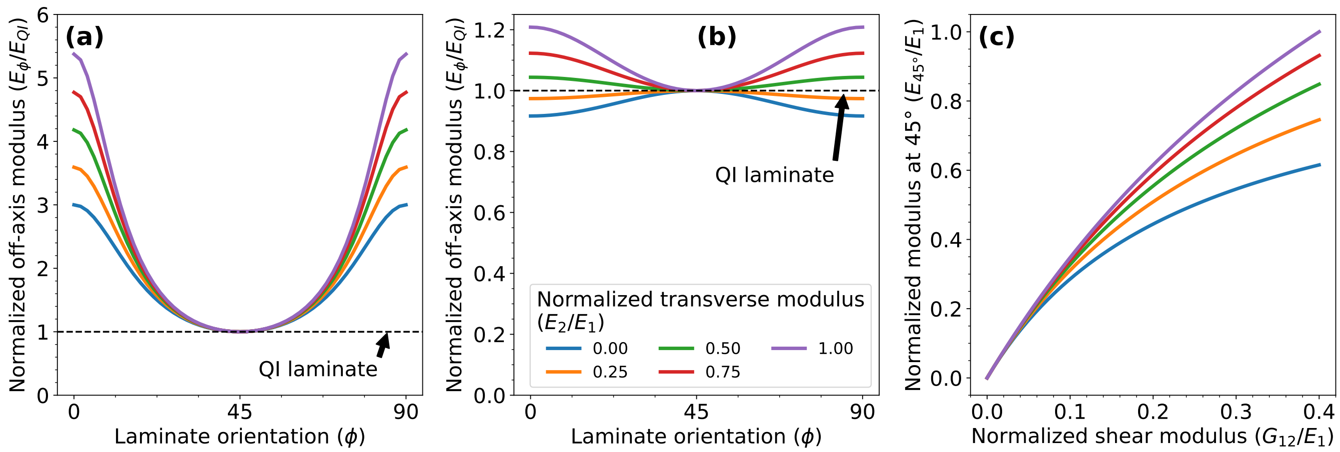

Figure 6. Lamina properties required to reach a target [0°/90°]s laminate Young's modulus, with $\nu_{12} = 0.25$ and (a) $G_{12} = 0.05$ or with (b) $G_{12} = 0.3$. (c) Relative laminate modulus at 45° relative to the lamina axial modulus with $\nu_{12} = 0.25$ for a [0°/90°]s laminate. Laminate orientations are indicated in degrees.

4 Relating fiber and matrix properties to lamina properties

The previous section describes the relationship between a laminate target and lamina requirements. In this section, the relationships between fiber properties, matrix properties, and lamina properties are investigated for fibers with ribbon cross sections.

The relationship between transverse lamina modulus and fiber volume fraction for various ratios of fiber transverse modulus and matrix shear modulus is shown in Figure 7. In Figure 7(a), the ratio of fiber to matrix stiffness is set to approximate a typical bio-based brick-and-mortar structure such as nacre [32]. For example, the blue curve (fiber volume fraction of 50%) replicates the conditions reported in Reference [32]. Some example fiber data are shown in Table 2, relative to the fiber axial modulus and relative to a baseline polymer matrix material. Some nanotube material properties in Table 2 are from as-received and stretched nanotube sheets [33]. Some of these sheets were processed using SPS which increased both the axial and transverse properties of the material. Relative to typical nacre ceramic/protein composites that can have $G_m/E_{f2} = 0.001$ (Figure 7(a)), carbon nanotube and carbon fiber reinforced polymer matrix composites have G_m/E_{f2} between 0.15–1.0 (Figure 7(b)-(d), Table 2). This greatly impacts the effect of fiber aspect ratio relative to conventional bio-based brick-and-mortar structures. For composites with G_m/E_{f2} between 0.15–1.0 the fiber cross-sectional aspect ratio is sufficient to transfer load at or below an aspect ratio of 10 as shown in Figure 7(b)-(d).

As the fiber volume fraction increases, the load is transferred over a shorter distance and aspect ratios less than five may be sufficient, depending on G_m/E_{f2}. Looking at a fixed fiber volume fraction of 80% (an approximate value of a "mortar" volume in the nanotube composite laminae), in Figure 8, as G_m/E_{f2} increases the load transfer occurs over a smaller portion of the fiber, and the aspect ratios that are required to maximize the lamina modulus are smaller.

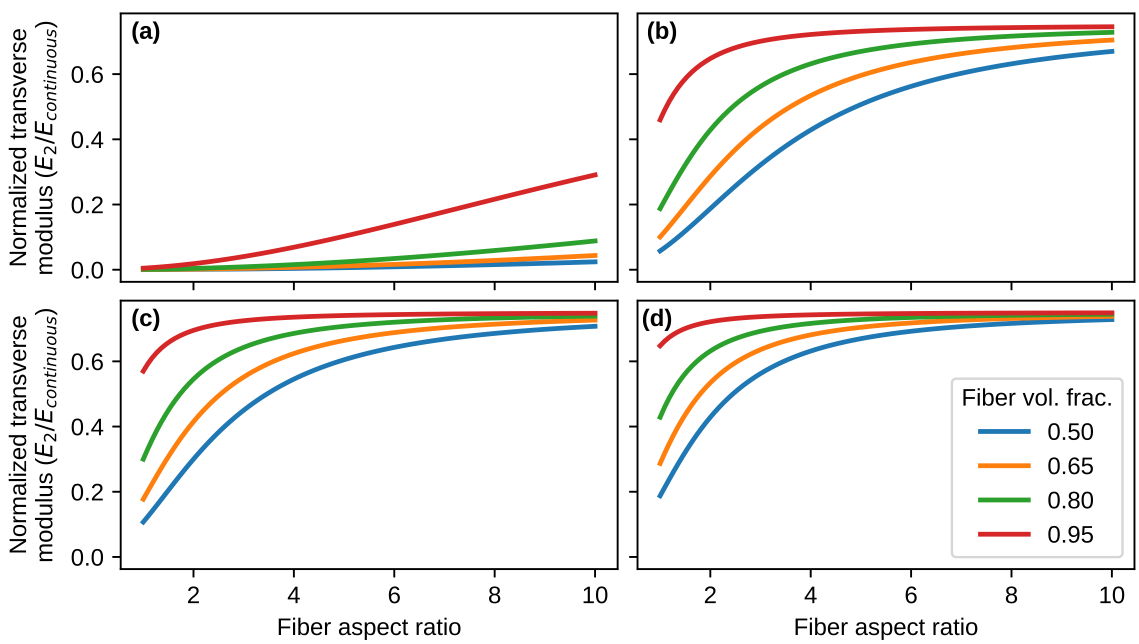

Figure 7. Lamina transverse modulus normalized against infinite aspect ratio (continuous sheet reinforcement) using brick-and-mortar micromechanics. (a) $G_m/E_{f2} = 0.001$, (b) $G_m/E_{f2} = 0.25$, (c) $G_m/E_{f2} = 0.5$, (d) $G_m/E_{f2} = 1$.

Looking at the lamina shear modulus in Figure 9, as the fiber volume fraction increases, there is marginal improvement until very high (>80%) fractions are reached. This is due to the assumption of equal shear stresses throughout the lamina, which results in an inverse rule of mixtures relationship. The maximum in-plane shear values are limited by the maximum shear modulus of the reinforcement. The lamina ν_{12} follows a straightforward standard rule of mixtures, and is not shown.

Table 2. Typical values of reinforcement engineering constants.

Material	**Normalized fiber transverse modulus (E_{f2}/E_{f1})**	**Normalized fiber shear modulus (G_{f12}/E_{f1})**	**Normalized matrix shear modulus (G_m/E_{f2})**	**Normalized fiber Poisson's ratio (ν_{f12})**	**Ref.**
Nanocomp carbon nanotube sheet 0% pre-strain	90%.	-	53%	-	[33]
Nanocomp carbon nanotube sheet 0% pre-strain w/SPS	77%.	-	15%	-	[33]
Nanocomp carbon nanotube sheet 43% pre-strain	17%.	-	105%	-	[33]
Nanocomp carbon nanotube sheet 43% pre-strain w/SPS	7.4%.	-	54%	-	[33]
Hexcel® IM7	5.4%.	9.8%	27%	0.28	[35]
Thornel® T-50	2.0%.	3.8%	53%	0.41	[36]
Thornel® T-300	12%.	22%	16%	0.44	[36]
Thornel® P-100	0.50%.	1.4%	120%	0.41	[36]
Thornel® T-700	6.5%.	10.4%	27%	-	[37]

† A representative polymer matrix with $E_m = 4$ GPa and $\nu_m = 0.4$ ($G_m = 1.45$ GPa) was used to compute this and other polymer dependent lamina engineering constants.

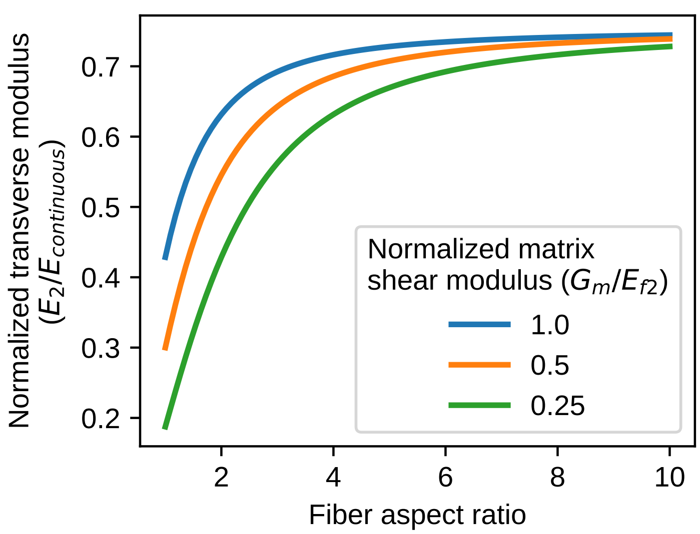

Figure 8. Lamina transverse modulus normalized against a fiber with an infinite aspect ratio (continuous sheet reinforcement) using brick-and-mortar micromechanics at a fixed fiber volume fraction of 80%.

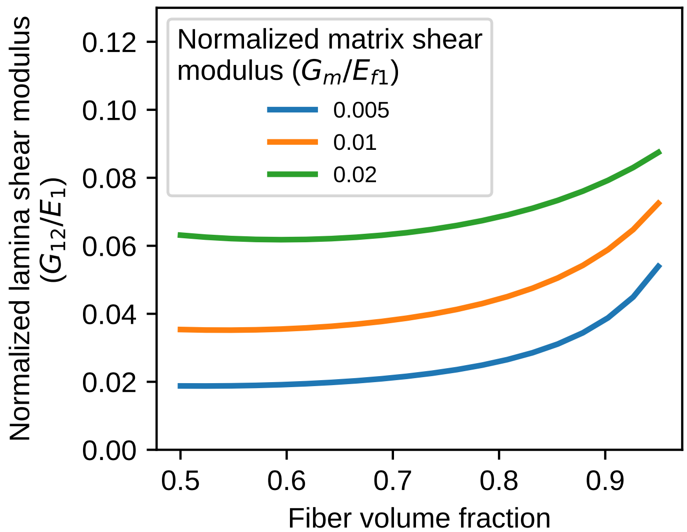

Figure 9. Lamina in-plane shear modulus normalized against the axial modulus for various fiber volume fractions and normalized matrix shear modulus.

5 Combined lamina and laminate analysis

In the previous two sections, the laminate requirements to reach a QI laminate target and the lamina constituent to lamina properties were investigated. Breaking the two length scales into separate analysis is typical of composite panel design for mature material systems with known constituent properties. Since this work is focused on material design, it is beneficial to combine the analysis so that the QI laminate target can be defined in terms of the fiber and matrix properties.

The options for designing a lamina from constituent properties are greater than designing lamina from a QI laminate target. For QI laminate to lamina there are three independent variables: E_1, E_2, and G_{12} (assuming the problem is not particularly sensitive to ν_{12}). However, for lamina, this doubles to six: E_{f1}, E_{f2}, G_{f12}, G_m, ρ, and V_f (again assuming ν insensitivity). The volume fraction can drive the constituent requirements. As the fiber volume fraction approaches zero, the fiber properties must approach infinity to meet the QI laminate target. Conversely, as the fiber volume fraction approaches one, the fiber properties approach the QI laminate target. Therefore, the minimum and maximum fiber axial modulus relative to a QI laminate target are computed for a discrete set of reasonably expected fiber volume fractions, with the results shown in Table 3, with the remaining dependent variables varied across a broad range as defined in the caption. For a relatively higher volume fraction of 0.9, the maximum fiber axial modulus is 3.2x the QI laminate target for a highly anisotropic fiber, while it can approach the QI laminate target as the fiber becomes isotropic. For a relatively lower fiber volume fraction of 0.6, the maximum fiber axial modulus requirement increases approximately 50% to 4.8x. So the fiber axial modulus can range between 1x and 4.8x the QI target, depending on the fiber anisotropy and volume fraction.

Visualizing and describing the design space for the six dimensional problem is challenging. To this end, a sensitivity analysis was performed with values ranging ±10% around values that are based on Hexcel® IM7/8552 but with a ribbon fiber and higher fiber volume fractions expected from a brick-and-mortar structure ($E_{f1} = 1$, $E_{f2} = 0.054$, $G_{f12} = 0.098$, $\rho = 10$, $G_m = 0.01458$, $V_f = 0.8$). This sensitivity analysis provides material designers with the slope of the multi-dimensional design space around a reasonably expected point based on IM7/8552. The results of the sensitivity analysis are shown in Figure 10.

Table 3. Fiber axial properties required to reach a QI laminate target. All remaining variable ranges are $0.05 < E_{f2}/E_{f1} < 1$, $0.05 < G_{f12}/E_{f1} < 0.5$, $0.05 < G_m/E_{f2} < 0.35$, $1 < \rho < 10$.

Fiber vol. frac.	**Normalized fiber axial modulus (E_{f1}/E_{QI})**	
	min	**max**
0.6	1.2	4.8
0.7	1.2	4.2
0.8	1.1	3.6
0.9	1.0	3.2

To perform the sensitivity analysis, a main-effects multiple linear regression analysis was performed on the dataset using the python package scikit-learn [38]. The material properties were normalized between 0–1 so that their relative impact on the Young's modulus of the QI panel can be compared.

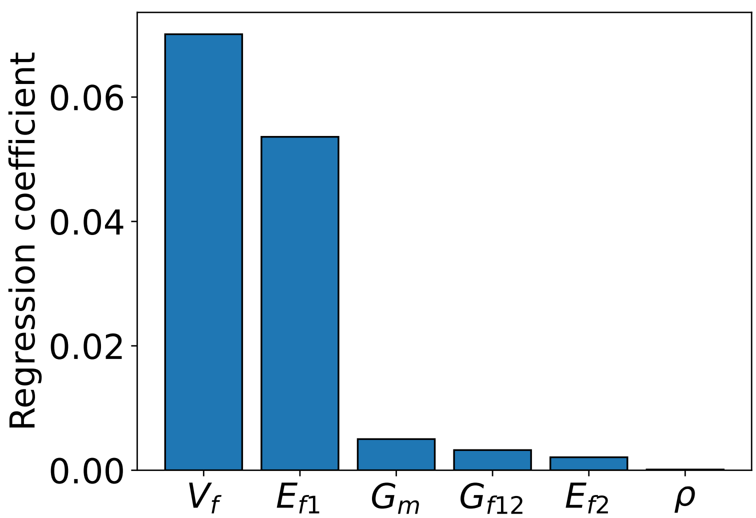

Figure 10. Ranked constituent property impact on a QI laminate with brick-and-mortar ribbon fibers.

The property with the largest impact on Young's modulus of the QI laminate is the fiber volume fraction. This is not surprising since both the axial and transverse Young's modulus benefit from increasing the volume fraction. Because of the ribbon fiber shape, it is possible to reach much higher fiber volume fractions than with round fibers, a potential advantage nanotube fibers may have over existing reinforcements. The next most impactful property is the fiber axial modulus, which is also not surprising since this is by far the highest mechanical property, so a 10% change represents the largest absolute change in properties.

The matrix shear modulus, transverse fiber modulus, and fiber aspect ratio are all related to the lamina transverse modulus. As was shown in the previous section, with a fiber aspect ratio of ten, the load transfer to the fibers is largely converged and small variations of 10% do not have a large impact.

6 Conclusions

In this work, the design space of carbon nanotube ribbon reinforced composites was investigated. Because nanotube fibers can have a ribbon cross section, the design space for lamina differs from most other fibers, which are typically round. Furthermore, laminate and lamina analysis typically involve mature material systems with established properties, and micromechanical analysis is performed to design laminate layups and predict performance for a set material system.

In this work, the objective was the inverse. This work focused on material design — to establish a laminate target requirement and perform an inverse micromechanical analysis to understand the design space of laminae and fiber properties that can be used to reach the target. The first section used classical lamination theory to investigate the lamina design space to reach a target QI laminate axial Young's modulus. The second section investigated the relationship between lamina constituent and lamina properties. Finally, in the third section, the two analyses were combined and the lamina constituent material properties were related to the QI laminate target.

The lamina axial modulus requirement ranges from a maximum of 3x to 1x minimum relative to the target QI laminate modulus depending on the anisotropy and shear modulus of the lamina. The fiber targets depend strongly on the fiber volume fraction in the lamina. The fiber axial modulus may be required to be a maximum of 4.8x the QI laminate target for a volume fraction of 0.6 or a maximum of 3.2x for a volume fraction of 0.9. Looking at the sensitivity of the requirements around a baseline IM7/8552 system (but with a brick-and-mortar structure with aspect ratio of ten and volume fraction of 0.8) the largest driver of performance was the volume fraction, followed by the fiber axial modulus. While bio-based brick-and-mortar composites, such as nacre, can benefit from reinforcement aspect ratios above 10, for carbon nanotube fiber (or carbon fiber) reinforced polymer matrix composites the difference between fiber transverse modulus and matrix shear modulus is orders of magnitude lower, resulting in cross-sectional aspect ratio requirements that are relatively smaller, potentially less than three.

Finally, this work used linear elastic material properties to investigate load transfer behavior of ribbon fibers. Elastic properties are an important component in the design of composite materials, along with failure and post-failure properties. While there may be correlations between the elastic properties studied here and failure and post-failure properties, more sophisticated computational techniques are required to gain a reasonable description of aspects of the design space of ribbon composites related to failure.

References

(1) J. A. Samareh and E. J. Siochi, *Nanotechnology*, 2017, **28**, 372001, DOI: 10.1088/1361-6528/aa7c5a.

(2) A. Pendashteh, A. Mikhalchan, T. Blanco Varela and J. J. Vilatela, *Discover Nano*, 2024, **19**, 208, DOI: 10.1186/s11671-024-04087-5.

(3) G. Gardiner, "Nanocomp Technologies Inc., Merrimack, NH, US", *Composites World*, July 7, 2016, https://www.compositesworld.com/articles/nanocomp-technologies-inc-merrimack-nh-us- (accessed 04/20/2026).

(4) L. W. Taylor, O. S. Dewey, R. J. Headrick, N. Komatsu, N. M. Peraca, G. Wehmeyer, J. Kono and M. Pasquali, *Carbon*, 2021, **171**, 689–694, DOI: 10.1016/j.carbon.2020.07.058.

(5) J.-W. Kim, J. M. Gardner, G. Sauti, R. A. Wincheski, B. D. Jensen, K. E. Wise and E. J. Siochi, *Composites Part A: Applied Science and Manufacturing*, 2023, **167**, 107449, DOI: 10.1016/j.compositesa.2023.107449.

(6) J. Thomason, A. Carlin and L. Yang, *Fibers*, 2024, **12**, 98, DOI: 10.3390/fib12110098.
(7) D. Edie, N. Fox, B. Barnett and C. Fain, *Carbon*, 1986, **24**, 477–482, DOI: 10.1016/0008-6223(86)90271-X.
(8) H.-B. Shim, M.-K. Seo and S.-J. Park, *Journal of Materials Science*, 2002, **37**, 1881–1885, DOI: 10.1023/A:1014959603892.
(9) S.-J. Park, M.-K. Seo and H.-B. Shim, *Materials Science and Engineering: A*, 2003, **352**, 34–39, DOI: 10.1016/S0921-5093(02)00463-X.
(10) G. Yuan, X. Li, Z. Dong, A. Westwood, B. Rand, Z. Cui, Y. Cong, J. Zhang, Y. Li, Z. Zhang and J. Wang, *Carbon*, 2014, **68**, 426–439, DOI: 10.1016/j.carbon.2013.11.019.
(11) I. Hanhan and M. D. Sangid, *Journal of Composites Science*, 2021, **5**, 294, DOI: 10.3390/jcs5110294.
(12) B. L. Ennis, H. S. Perez and R. E. Norris, *Materials Today Communications*, 2022, **33**, 104298, DOI: 10.1016/j.mtcomm.2022.104298.
(13) "CPIC develops family of unique fiberglass products", *Composites World*, January 15, 2018, https://www.compositesworld.com/news/cpic-develops-family-of-unique-fiberglass-products (accessed 04/20/2026).
(14) J. Halpin and R. Thomas, *Journal of Composite Materials*, 1968, **2**, 488–497, DOI: 10.1177/002199836800200409.
(15) J. C. Halpin and J. L. Kardos, *Polymer Engineering and Science*, 1976, **16**, 344–352, DOI: 10.1002/pen.760160512.
(16) J. Rexer and E. Anderson, *Polymer Engineering & Science*, 1979, **19**, 1–11, DOI: 10.1002/pen.760190102.
(17) J.-W. Kim, J. M. Gardner, G. Sauti, B. D. Jensen, R. A. Wincheski, J. G. Smith, S. R. Zavada, K. E. Wise and E. J. Siochi, *Multiple Mechanical Behaviors of Carbon Nanotube Fiber Reinforced Epoxy Composites*, NASA/TM–20250008896, 2025, DOI: 10.64631/GXFM8692.
(18) S. Askarinejad and N. Rahbar, *Journal of The Royal Society Interface*, 2015, **12**, 20140855, DOI: 10.1098/rsif.2014.0855.
(19) A. Bahmani, G. Li, T. L. Willett and J. Montesano, *Composite Structures*, 2019, **212**, 484–499, DOI: 10.1016/j.compstruct.2019.01.056.
(20) M. Mirkhalaf and H. Zreiqat, *JOM*, 2020, **72**, 1458–1476, DOI: 10.1007/s11837-019-03986-8.
(21) S. Morsali, D. Qian and M. Minary-Jolandan, *Communications Materials*, 2020, **1**, 12, DOI: 10.1038/s43246-020-0012-7.
(22) S. Pimenta and P. Robinson, *Composites Science and Technology*, 2014, **104**, 111–124, DOI: 10.1016/j.compscitech.2014.09.001.
(23) X. Gao, X. Lu, X. Zhang, M. Qian, A. Li, H. Wang, C. Liu, B. Gong, W. Ouyang and H.-X. Peng, *Applied Composite Materials*, 2024, **31**, 1457–1473, DOI: 10.1007/s10443-024-10221-4.
(24) J. Henry and S. Pimenta, *Journal of the Mechanics and Physics of Solids*, 2018, **118**, 322–340, DOI: 10.1016/j.jmps.2018.06.003.
(25) V. Rajan and W. Curtin, *Journal of the Mechanics and Physics of Solids*, 2016, **90**, 1–17, DOI: 10.1016/j.jmps.2016.02.011.

(26) T. P. Niebel, F. Bouville, D. Kokkinis and A. R. Studart, *Journal of the Mechanics and Physics of Solids*, 2016, **96**, 133–146, DOI: 10.1016/j.jmps.2016.06.011.

(27) M. R. Begley, N. R. Philips, B. G. Compton, D. V. Wilbrink, R. O. Ritchie and M. Utz, *Journal of the Mechanics and Physics of Solids*, 2012, **60**, 1545–1560, DOI: 10.1016/j.jmps.2012.03.002.

(28) R. F. Gibson, *Principles of composite material mechanics*, ISBN: 978-0-07-023451-2, CRC Press, 2016.

(29) Hypersizer, *HyperX*, 2025.

(30) A. T. Nettles, *NASA-RP-1351*, 1994.

(31) J.-W. Kim, G. Sauti, B. D. Jensen, J. G. Smith, K. E. Wise, R. A. Wincheski, R. J. Cano and E. J. Siochi, *Carbon*, 2021, **173**, 857–869, DOI: 10.1016/j.carbon.2020.11.055.

(32) Z. Zhang, B. Liu, Y. Huang, K. Hwang and H. Gao, *Journal of the Mechanics and Physics of Solids*, 2010, **58**, 1646–1660, DOI: https://doi.org/10.1016/j.jmps.2010.07.004.

(33) B. D. Jensen, J.-W. Kim, G. Sauti, K. E. Wise, L. Dong, H. N. G. Wadley, J. Gyu, R. Liang and E. J. Siochi, *Carbon*, 2020, **156**, 538–548, DOI: 10.1016/j.carbon.2019.09.090.

(34) K. Marlett, *Hexcel 8552 IM7 Unidirectional Prepeg 190 gsm & 35%RC Qualification Material Property Data Report*, CAM-RP-2009-015 Rev A, 2009.

(35) E. Zeitunian, Master of Science in Mechanical Engineering, Michigan Technological University, Houghton, Michigan, 2022, DOI: 10.37099/mtu.dc.etdr/1387.

(36) National Aeronautics and Space Administration, *MAC/GMC 4z-3.11*, version 4z-3.11, 2002.

(37) X. Li, W. K. Binienda and R. K. Goldberg, *Journal of Aerospace Engineering*, 2011, **24**, 170–180, DOI: 10.1061/(ASCE)AS.1943-5525.0000029.

(38) F. Pedregosa, G. Varoquaux, A. Gramfort, V. Michel, B. Thirion, O. Grisel, M. Blondel, P. Prettenhofer, R. Weiss, V. Dubourg, J. Vanderplas, A. Passos, D. Cournapeau, M. Brucher, M. Perrot and E. Duchesnay, *Journal of Machine Learning Research*, 2011, **12**, 2825–2830.